Materials Science & Engineering A 819 (2021) 141408

Contents lists available at ScienceDirect

Materials Science & Engineering A

journal homepage: www.elsevier.com/locate/msea

Deformation mechanisms of basal slip, twinning and non-basal slips in Mg–Y alloy by micropillar compression

Na Li [a,b], Lingwei Yang [c,*], Chuanyun Wang [d], M.A. Monclús [b], Dongfeng Shi [b,e], J.M. Molina-Aldareguía [b,**]

[a] LNM, Institute of Mechanics, Chinese Academy of Sciences, Beijing, 100190, China
[b] IMDEA Materials Institute, C/Eric Kandel 2, 28906, Getafe, Madrid, Spain
[c] Hypervelocity Aerodynamics Institute, China Aerodynamics Research and Development Center, Mianyang, 621000, China
[d] State Key Laboratory of Solidification Processing, Northwestern Polytechnical University, Xi'an, 710072, China
[e] Department of Materials Science, Polytechnic University of Madrid/Universidad Politécnica de Madrid, E. T. S. de Ingenieros de Caminos, 28040 Madrid, Spain

ARTICLE INFO

Keywords:
Magnesium alloy
Mechanical property
Micropillar compression
Deformation mechanisms

ABSTRACT

Micropillar compression technique was employed to study the microscale deformation mechanisms of basal slip, twinning and non-basal slips at selected grains in a Mg-2 wt.% Y alloy. The results suggest a critical resolved shear stress (τCRSS) for basal slip 12.5 ± 1.7 MPa, and for twin nucleation and twin growth 38.5 ± 1.2 MPa and 33.8 ± 0.7 MPa, respectively. The higher values compared to those in pure Mg suggests a more balanced deformation in Mg alloy with Y addition. The activation of <c+a> dislocations in the twinned orientation is highlighted, which leads to strong work hardening in twinned favorable orientation [10$\bar{1}$0]. In addition, at prismatic-slip favorable orientation [11$\bar{2}$0], a twinning-to-prismatic slip transition was observed when elevating temperature from 25 °C to 100 °C and 250 °C. Specially at 250 °C, twinning was completely prohibited, and pure prismatic slip was triggered. The measured τ_{CRSS} for prismatic slip at 250 °C was 39.7 ± 0.3 MPa, much higher than that for pure Mg at the same temperature. Finally, at pyramidal-slip favorable orientation [0001], an abnormal strengthening was observed at 100 °C and 250 °C due to activation of pyramidal slips. Decompositions of <c+a> dislocations and Y segregation at stacking faults are the main mechanisms leading to the high-temperature strengthening in Mg–Y alloy.

1. Introduction

Magnesium (Mg) and its alloys have been widely applied in vehicles, electronics, medical equipment, et al., due to their high specific strength, low density and biodegradable properties. As atomic lattice of Mg is hexagonal close-packed (hcp) structured, the mechanical performance of Mg alloys is still limited by the strong plastic asymmetry, poor deformability and high temperature sensitivity [1–5]. At microscale, the deformation of Mg is coupled contributions of 4 independent activities, including basal slip, twinning and non-basal slips (pyramidal and prismatic slips). The difference in the critical resolved shear stress (τ_{CRSS}) and their temperature sensitivity mainly dominate the mechanical performance of Mg alloys at room temperature (RT) and high temperatures (HT). E.g., τ_{CRSS} of basal slip in pure Mg is only ≈0.5 MPa at RT [6–8], which is much lower than that of non-basal slips (≈40 MPa) [9–11]. As a result, sharp basal textures preferentially form during deformation of Mg. They are detrimental to the formability and ductility of Mg alloy. As basal slip only provides 2 independent slip systems, synergistic deformation of Mg still necessitates another deformation along $<c>$ axis, and this is generally accommodated by twinning in Mg. Twinning emerges under uniaxial compression (leading to strong tension-compression asymmetry), and the τ_{CRSS} for twinning is ≈ 12 MPa at RT. The large differences in the τ_{CRSS} of basal slip, twinning and non-basal slips thus lead to strong mechanical anisotropy of Mg alloys at RT. At HT, the mechanical anisotropy of Mg is markedly reduced, especially at $0.4T_m$ (melting point). It is found that non-basal slips become more operative at HT due to the reduced τ_{CRSS}. However, the reduction in the τ_{CRSS} of non-basal slips may degrade strongly the strength of Mg at HT. For instance, in AZ31 Mg alloys, the yield strength at 200 °C was only ≈89 MPa, which was much lower than that at RT ≈ 155 MPa [12].

* Corresponding author.
** Corresponding author.
E-mail addresses: lingwei.yang@cardc.cn (L. Yang), jon.molina@imdea.org (J.M. Molina-Aldareguía).

https://doi.org/10.1016/j.msea.2021.141408
Received 28 August 2020; Received in revised form 21 March 2021; Accepted 30 April 2021
Available online 18 May 2021

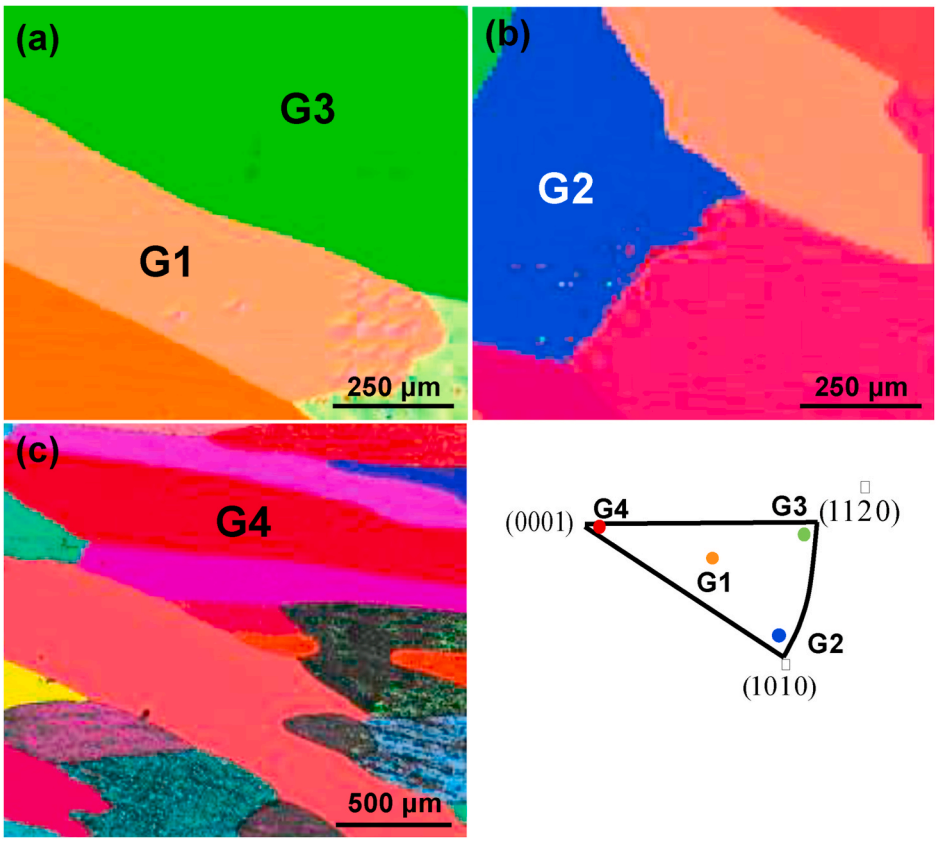

Fig. 1. (a, b, c) Derived inverse pole figure (IPF) maps of the grain 1 to grain 4 in Mg–2Y alloy, based on the EBSD measurement.

The large τ_{CRSS} difference in Mg can be reduced by alloying with rare earth (RE) elements, which gives rise to toughness enhancement and temperature resistance of Mg alloys [13,14]. Recent studies show that the fracture elongation of a Mg-3 wt.% Y alloy was ≈0.25 at RT, 5 times higher than that of pure Mg (≈0.05) [15]. The toughening mechanisms lie in the balanced τ_{CRSS} between basal and non-basal slips and the activations of $<c+a>$ dislocations that provide more than 5 independent slip systems. At HT, due to segregation of Y elements along grain boundaries and solute drag effects, the degradation of strength in Mg–Y alloys was effectively retarded at HT [16]. Despite this, the current study on deformation mechanism of Mg–Y alloy is still limited at macroscale where the polycrystalline grains and grain boundaries play a dominant role. The individual slip mechanisms and the τ_{CRSS} of basal slip, twining and non-basal slips are still unknown at both RT and HT, which information is important to understand the orientation and temperature dependent deformations in Mg–Y alloys.

To this end, in this work micropillar compression technique was employed to study the deformation mechanisms of basal slip, twinning and non-basal slips of a typical Mg-2 wt.% Y (Mg–2Y) alloy at microscale. As the test was uniaxial compression, 4 grains oriented at [11$\bar{2}$3], [10$\bar{1}$0], [11$\bar{2}$0] and [0001] were positioned on a finely polished cross-section by electron backscatter diffraction (EBSD) technique. Among them, the [11$\bar{2}$3] and [10$\bar{1}$0] were basal slip and twinning favorable orientations. The inside micropillars were thus tested at RT, as both activities were thermally independent [17]. The [11$\bar{2}$0] and [0001] were prismatic and pyramidal favorable orientations, specifically at HT, thus the micropillars inside were compressed at RT, 100°C and 250°C, in order to trigger the non-basal slips and to study the temperature sensitivity. After micropillar compressions, scanning and transmission electron microscopies (SEM & TEM) and transmission Kikuchi diffraction (TKD) were used to provide insight on slip and dislocation activities. Based on the shear stress-strain curves of each orientation, τ_{CRSS} of basal slip, twinning and non-basal slips in the Mg–2Y were finally derived to forward fundamental understanding of the orientation and temperature dependent mechanical behavior.

2. Materials and experimental techniques

The Mg–2Y alloy was manufactured by casting technique using high-purity Mg and Y particles inside an induction furnace (VSG 002 DS, PVA TePla) in Ar atmosphere. The cast ingots were homogenized at 400 °C for 7 days to achieve a homogeneous composition and also to induce grain growth. The surfaces of the Mg–2Y alloys were mirror-polished using standard metallographic techniques [18]. The microstructure of the as-casted Mg–2Y was characterized by SEM (Helios Nanolab 600i FEI, supplemented as Fig. S5) and EBSD (Oxford Instruments

Table 1
The maximized SFs (m) of the selected grains.

Grain	Orientation	Loading direction	Basal slip	Prismatic slip	Pyramidal slip	Tension twinning
G1	(76.0°, 42.5°, 48.1°)	[11$\bar{2}$3]	0.48	0.22	0.29	0.26
G2	(61.8°, 94.8°, 24.2°)	[10$\bar{1}$0]	0.07	0.47	0.39	0.49
G3	(91.8°, 94.0°,157.7°)	[11$\bar{2}$0]	0.07	0.45	0.4	0.39
G4	(24.1°, 172.1°, 49.1°)	[0001]	0.13	0.37	0.49	–

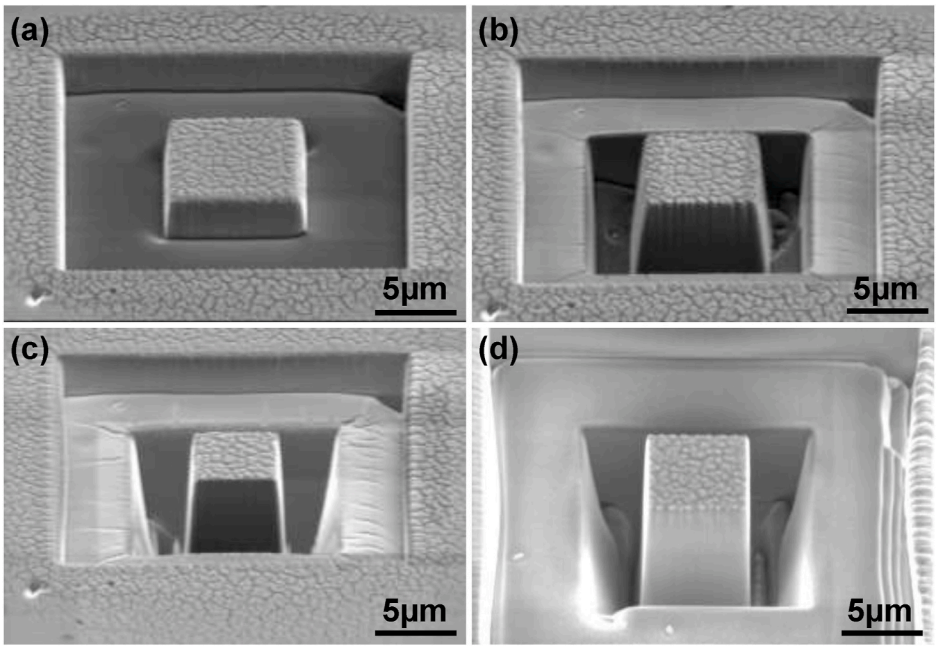

Fig. 2. FIB milling protocol of a typical micropillar in Mg–2Y alloy: (a) rough milling with 21 nA ion current; (b) fine milling with 9.3 nA ion current; (c) tapper removal; (d) final shaped micropillar.

NordlysNano electron). The EBSD measurements were carried out at 30 kV accelerating voltage and 2.7 nA beam current, using a step size of 5μm. The acquired data was analyzed by the Aztec and Channel 5.0 software package. Four typical grains oriented at $[11\bar{2}3]$, $[10\bar{1}0]$, $[11\bar{2}0]$ and [0001] were positioned for micropillar compression tests, as shown in Fig. 1. They are labeled as G1, G2, G3 and G4 in this work. Note the selected grains were large enough for the micropillar fabrications. Based on the grain orientation, the Schmid factors (m) for basal slip, twinning, pyramidal slip and prismatic slip of the 4 grains were calculated according to Ref. [19]:

$$m = \cos(\varphi) \times \cos(\lambda) \tag{1}$$

where φ is the angle between the applied stress and the normal to the slip plane, and λ is the angle between the applied stress and slip direction. The calculated m of the 4 orientations are listed in Table 1.

Micropillar compression was performed in the selected grains (G1∼G4) of the Mg–2Y alloy. Prior to that, square cross-sectioned micropillars were milled by focused ion beam (FIB) technique inside a Helios Nanolab 600i SEM/FIB dual beam system. The ion source was Ga^+, and the accelerating ion voltage was 30 kV. Fig. 2 shows a typical milling protocol of the square micropillar in Mg–2Y alloy at a tilted angle of 52° (ion gun vertical to the milling surface). At the sites of the selected grains, the following successive milling steps were carried out: (i) rough milling to fast remove the surrounding material by using a very high ion current (24 nA) (ii) milling with smaller ion currents (i.e., 9.3 and 2.5 nA); to smoothly approach the target dimension (size length 5 μm and 7 μm, aspect ratio in the range 2:1 to 3:1); (iii) taper removal and surface polishing with an 80 pA ion current by overtilting the sample stage to 53.5°and 50.5°, respectively; (iv) 90° stage rotation and repetition of step (iii). 2 types of micropillars with cross-sections of $5 \times 5\ \mu m^2$ and $7 \times 7\ \mu m^2$ were milled inside each grain, in order to ascertain the micropillar size effect. Note the size effect arises in Mg alloy at micron scales due to dislocation starvation [20,21]. Generally, a 'the smaller, the stronger' rule was observed in Mg alloy [21,22]. Therefore, it is important to study the micropillar size effect in priority and to determine the micropillar dimension that is representative. Extensive studies suggest that when the edge size is ≥ 7 μm, the size effect is negligible [20–22]. This is also the case for the micropillar in Mg–2Y alloys (see Supplementary Fig. S1). Therefore, only the representative curves of each orientation were plotted in the following sections.

The as-milled micropillars were compressed using standalone Hysitron TI950 Triboindenter (RT test) and PI87 Picoindenter equipped inside a SEM system (ZEISS EVO18, HT test). Details of both micromechanical facilities are provided as supplementary information (Figs. S2 and S3). Note the SEM system provides a high vacuum environment (vacuum $< 1 \times 10^{-5}$ Pa), which is important for HT micropillar compressions as potential oxidations were eliminated. A diamond flat punch (diameter = 10 μm) was used for all experiments. The misalignment between the flat punch and the top surface of the micropillars was carefully corrected in these tests. All the tests were implemented under displacement-control mode at an average strain rate of $10^{-3}\ s^{-1}$ up to a maximum strain of 10%. The acquired load-displacement curves were corrected to account for the compliance due to elastic deflection of Mg–2Y beneath the micropillars, based on Sneddon's correction model [23,24]. The corrected force and displacement were converted to engineering stress (σ)-strain (ε) based on:

$$\sigma = \frac{P}{A_0} \tag{2}$$

$$\varepsilon = \frac{D}{L_0} \tag{3}$$

Here, P and D are the corrected load and displacement after Sneddon's correction. A_0 and L_0 are the initial cross-section and height of the micropillars. Based on the σ-ε curves, the yield stress (σ_{yield}) of each orientation was determined and τ_{CRSS} of basal slip, twinning and non-basal slips were finally calculated based on:

$$\tau_{CRSS} = m \cdot \sigma_{yield} \tag{4}$$

After the micropillar compression tests, the slip traces emerged on the free surface of the micropillars were characterized by SEM. They are key information to determine the activated slip systems, thus to trace the deformation histories. In order to gain insight in the dislocation activities, thin lamellas of ≈100 nm in thickness were trenched and lifted-out from deformed micropillars for further TEM characterization (Talos F200X FEI). In current study, bright field imaging (BF) and selected area diffraction (SAD) were utilized to characterize the twinning deformation

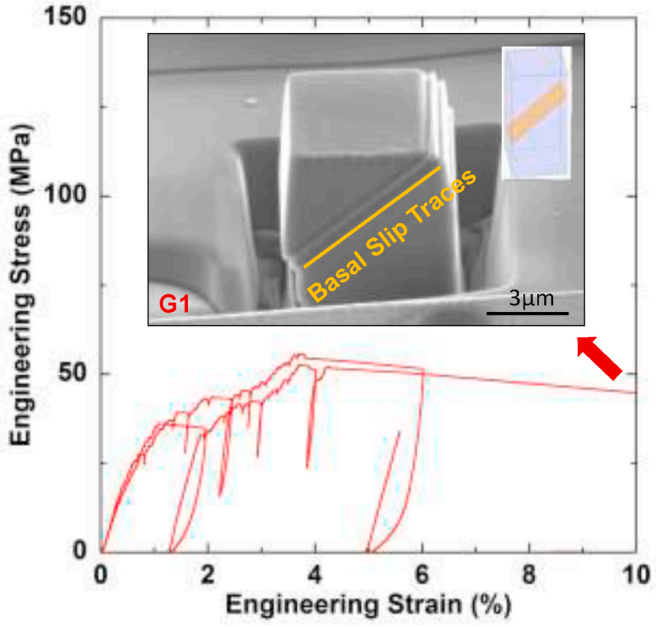

Fig. 3. Compressive stress-strain curves of the micropillars at RT in basal favorable (G1) orientation. The insert is a typical compressed micropillar.

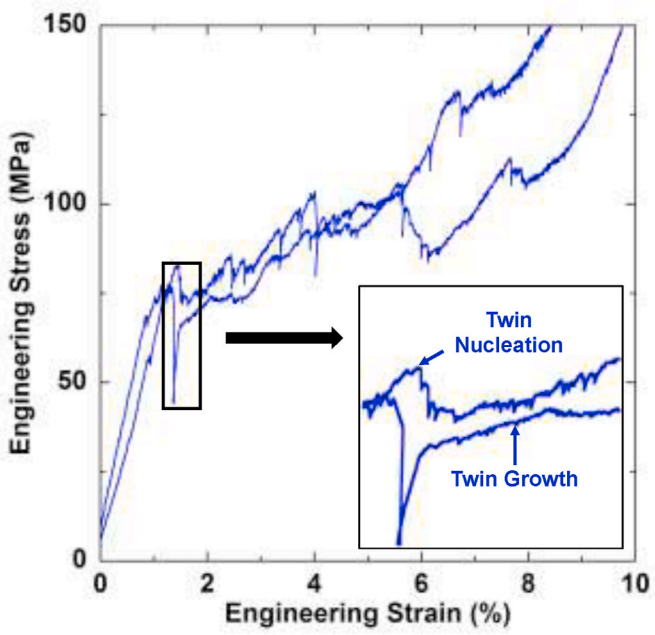

Fig. 4. (a) Compressive stress-strain curves of the micropillars in twinning favorable (G2) orientations.

Table 2
Measured τ_{CRSS} for basal slip, twinning, prismatic and pyramidal slips in Mg–2Y alloy.

Slip Mode	τ_{CRSS}		
	25 °C	100 °C	250 °C
Basal Slip	12.5 ± 1.7	–	–
Twin Nucleation	38.5 ± 1.2	–	–
Twin Growth	33.8 ± 0.7	–	–
Prismatic Slip	–	–	39.7 ± 0.3
Pyramidal slip	–	43.7 ± 0.3	45.6 ± 0.7

upon micropillar compression. Based on the diffraction patterns, the orientation relationship between twinning and matrix was deternmined. In order to identify basal and non-basal dislocations, two-beam dark-field (DF) TEM mode with $g = (0002)$ was used to characterize the non-basal triggered dislocation. i.e., <c+a> dislocations, based on dislocation visibe rule $g{\cdot}b \neq 0$.

3. Results and discussion

3.1. Deformation mechanism of basal slip

As the micropillars of G1 and G2 were oriented for basal slip and tensile twinning favorable modes, they were firstly tesed at RT. The HT micropillar compressions were not performed since basal slip and twinning were temperature insensitive. Fig. 3 plots the engineering stress-strain curves of the micropillars compressed in G1. Since m for basal slip in G1 was 0.48 (Table 1), higher than that of the rest slip modes, basal slip was preferientially activated at this orientation ($[11\bar{2}3]$). This deformation mode was further supported by detailed SEM observation of the micropillar, insert in Fig. 3. Basal slip traces that were formed by shearing of single set of parallel slip planes were observed on the lateral surface of the micropillar. The typical stress-strain curve for this grain began with an elastic deformation, which was followed by a pronounced plastic yielding. The yield stress was 25.0 ± 3.5 MPa, and this led to a τ_{CRSS} for basal slip 12.5 ± 1.7 MPa based on Eq. (4), as listed in Table 2. The value agrees well with the reported τ_{CRSS} for basal slip in Mg-2.2 wt% Y [25]. Note compared to the τ_{CRSS} for pure Mg (≈5.0 MPa), the enhanced τ_{CRSS} for basal slip in Mg–2Y alloy can be explained by the solute misfit volume and stacking fault energies [26]. Note multiple stress drops were also observed as deformation proceeded, and this phenomena is mainly a consequence of activation of dislocation slips.

3.2. Deformation mechanism of tensional twinning

The slip activities were quite different in the micropillar of G2. At this orientation ($[10\bar{1}0]$), m for twinning was 0.49 (Table 1), therefore tensional twinning was preferientially activated. Fig. 4 plots the engineering stress-strain curves of the micropillar at RT. Sudden drop in the stress level occurred at ≈1.5% applied strain, and this was a consequence of twin nucleation [27,28]. Following that, the twin was propagated through the entire micropillar, as indicated by a strain plateau in the curve (insert in Fig. 4). Based on the yield stress level for twinning, τ_{CRSS} for twinning nucleation and twinning growth were calculated 38.5 ± 1.2 MPa and 33.8 ± 0.7 MPa, respectively, based on Eq. (4) (Table 2). Note the values were enhanced significantly, compared to those in pure Mg (≈20.0 MPa and ≈16.5 MPa) [29]. This result highlights that the addition of Y can strengthen remarkably the tensional twinning deformation. Accordingly, the ratio of τ_{CRSS} for twinning nucleation to τ_{CRSS} for basal slip was ≈3 in Mg–2Y alloy, much lower than that in pure Mg (≈4). This suggests a more balanced deformation in Mg–Y alloy.

The twin formation was successfully observed by TKD in a thin lamellae of the compressed micropillar. Fig. 5 (a) shows the BF-TEM of the lamellae and (b) presents the corresponding TKD contour. The matrix domain was only observed at upperpart of the micropillar, beneath it was a large area of twin domain. Detailed SADPs of both domains are shown in Fig. 5(c–d). At zone axis of $\langle 10\bar{1}0\rangle$, the c-axis ([0001]) in the matrix (green line, Fig. 5c) was almost vertical to that in the twin (blue line, Fig. 5d). This evidences that the lattice in the matrix was rotated for ≈90° to form the twin, thus the orientation was changed from $[10\bar{1}0]$ to [0001] (c-axis). TKD results show an Euler angle of the twin orientation (15°, 85.3°, 26.9°), which gives m for basal, prismatic and pyramidal slips 0.24, 0.01 and 0.49, respectively. Though the twin orientation was not optimized for basal slip (due to low m, compared to that in G1), basal slip was still activated. This was evidenced from the traces formed on the surfaces of the deformed micropillar. As shown in Fig. 5 (e), the traces

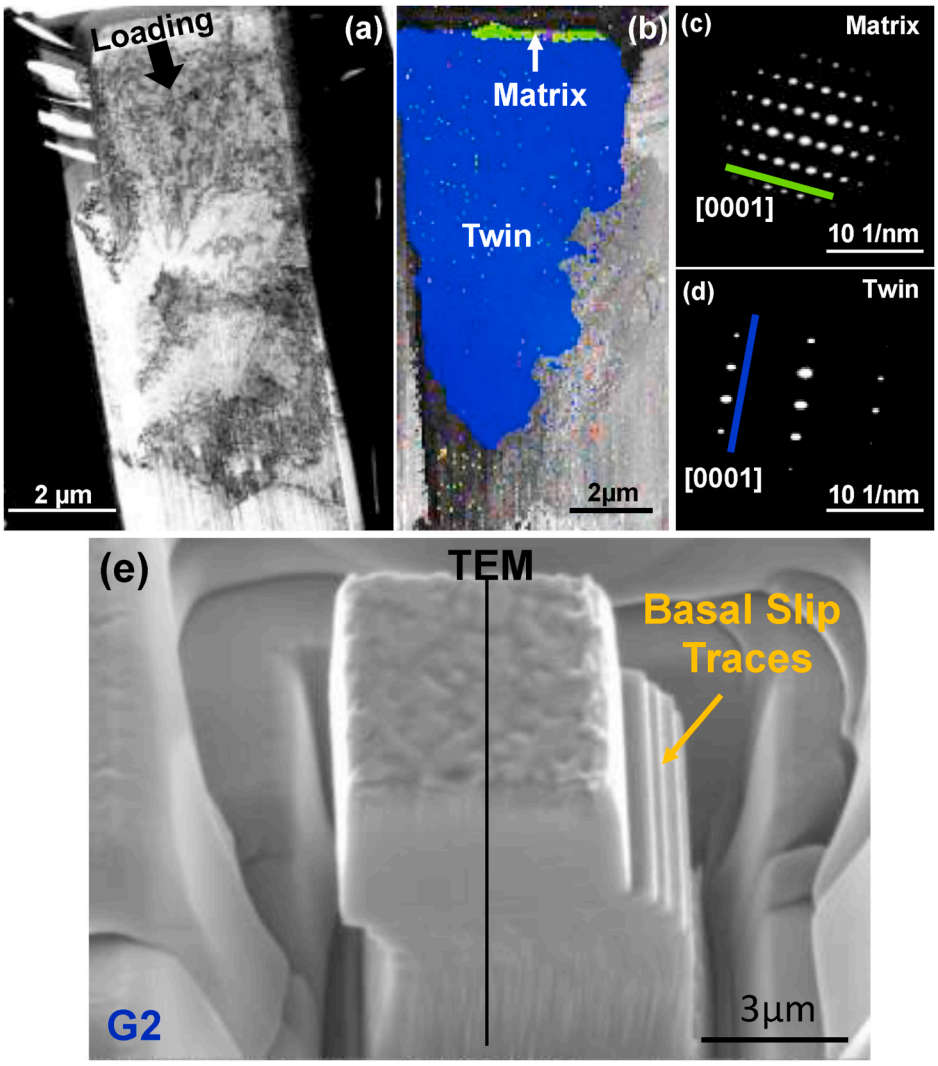

Fig. 5. Microstructure of a typical deformed micropillar in G2: (a) BF-TEM image; (b) TKD image; (c, d) SADPs of matrix and twin domain; (e) SEM image.

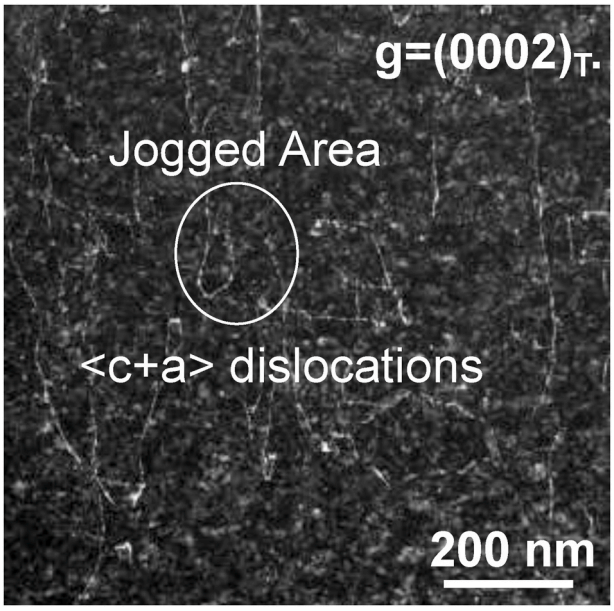

Fig. 6. DF-TEM in the deformed micropillar in G2 under two-beam mode with $\bar{g} = (0002)_T$.

were vertical to the loading direction ([0001] for the twin). The formation of them could be only a consequence of basal slip, since non-basal slips were inclined to the c-axis.

Prismatic slip was also triggered in the twin, considering the high *m* for the twin orientation. Though the traces of prismatic slip were hardly observed from the slip traces, the deformation can be still evidenced by the formation of $<c+a>$ dislocations. $<c+a>$ dislocation has a burgers vector (b)of $[11\bar{2}3]$. It can be tracked by two-beam mode in TEM, based on $g \cdot b \neq 0$ E.g., giving $g = (0002)_T$, the $<c+a>$ dislocations were visible and $<a>$ dislocations due to basal slip ($\bar{b} = [1\bar{2}10]$, $[11\bar{2}0]$, $[2\bar{1}\bar{1}0]$) were not visible. Thus, the observed dislocations in Fig. 6 belonged to $<c+a>$ dislocations. They were entangled and interacted with $<a>$ dislocations (in the basal plane), thus forming large density dislocation jogs in the twin. This dislocation activity well explains the strong strain hardening behavior of the micropillar after twin formation (Fig. 4).

3.3. Deformation mechanism of prismatic slips

Compared to the orientations in G1 and G2, *m* for prismatic slip in G3 and pyramidal slip in G4 were both high (0.45 and 0.49), the non-basal slips probably occurred at both orientations at HT. Therefore, micropillar compressions were performed at RT, 100 °C and 250 °C in G3 and G4, to study the deformation mechanism of the non-basal slips. Fig. 7

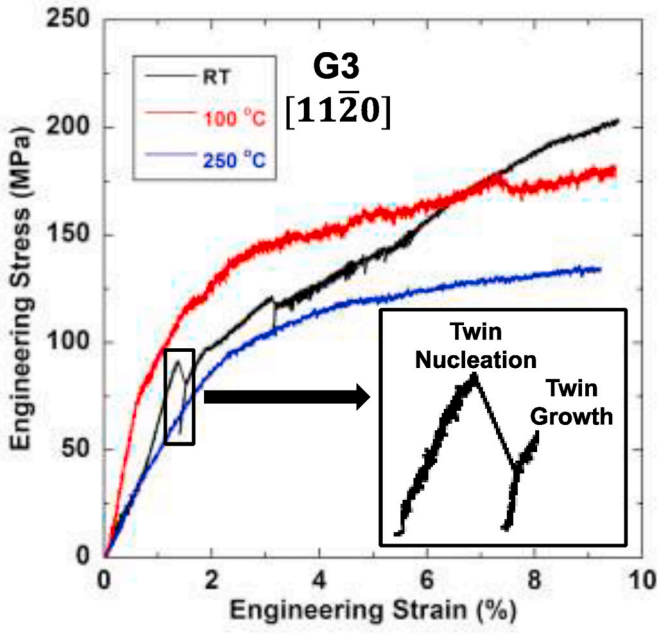

Fig. 7. Engineering stress-strain curves of micropillars at RT, 100 °C and 250 °C in G3.

shows the typical stress-strain curves of G3 orientation at RT, 100 °C and 250 °C. Though *m* for prismatic slip was higher than that for twinning in G3 orientation (0.45 vs. 0.39), twinning was still prone to occur at RT, due to the comparably low τ_{CRSS} (≈38.7 MPa for twin nucleation section 3.1). In the stress-strain curve (black curve, Fig. 7a), sudden drops in the stress level and the following work hardening were much similar to the scenario observed in G2 (Fig. 4) and was mainly a consequence of twin nucleation/growth and dislocation jog formations (Fig. 6). Similar basal slip traces in the twined regime were also observed on the lateral surfaces of the deformed micropillar, as shown in Fig. 8 (a), in accordance with that in G2 (Fig. 5e). The calculated τ_{CRSS} for twin nucleation and growth based on the RT curve in G3 was ≈35.1 MPa and ≈31.6 MPa, respectively, similar to those obtained in G2. This verifies the validity of the derived τ_{CRSS} for twinning in the Mg–2Y alloy.

The stress-strain curve was rather smooth at 100 °C and 250 °C, signifying the prohibition of twinning activity at HT. Despite this, twinning was still activated at 100 °C, as evidenced by the emergence of basal slip traces on the deformed micropillar (Fig. 8b). Except for the basal slip traces, wavy traces inclined to the loading direction were also observed. As G3 was oriented for prismatic slip, they were formed mainly by prismatic slip. Therefore, at 100 °C twinning and prismatic slip coexisted. Twinning was completely prohibited at 250 °C. Based on the stress-strain curve, the yield stress at 250 °C was ≈85 MPa, lower than that at RT (≈90 MPa) for twinning activation. The stress level was not high enough to trigger twinning, especially at the initial yielding stage. The sole prismatic deformation at this temperature was further supported by the vanishing of basal slip traces and emergence of prismatic slip traces on the lateral surfaces of the micropillar. Based on the measured yield stress values at 250 °C, the τ_{CRSS} for prismatic slip was 39.7 ± 0.3 MPa, as listed in Table 2. This is the first successful measurement of the τ_{CRSS} for prismatic slip in Mg–Y system. Note the τ_{CRSS} for prismatic slip in pure Mg was ≈32 MPa at RT, and was reduced to only ≈8 MPa at 300 °C. The much higher τ_{CRSS} value in Mg–Y alloy suggests that the Y addition aided further strengthening in Mg alloy, especially at HT [30,31].

3.4. Deformation mechanism of pyramidal slips

G4 was oriented close to [0001] c-axis, and the micropillars showed a rather different temperature dependent response. Fig. 9 plots the compressive stress-strain curves of G4 micropillars at RT, 100 °C and 250 °C. At this orientation, basal slip was still activated at RT, leading to a low level of yield strength (≈25 MPa) and weak work hardening behavior. The compressive response was similar to that in G1 (see Fig. 3). The parallel traces emerged on the surfaces of the deformed micropillar further suggest the activation of basal slip at RT, as shown in Fig. 10 (a). Since basal slip was temperature independent, it was also activated at 100 °C, as evidenced by the comparable yield stress and analogous basal slip traces, Fig. 10 (b). Unlike the stress-strain curve at RT, the strain hardening rate at 100 °C was higher, and an abrupt stress burst was still observed at ≈ 6% applied strain (indicated by the red arrow). This manifests the activation of other slip activities, i.e.,

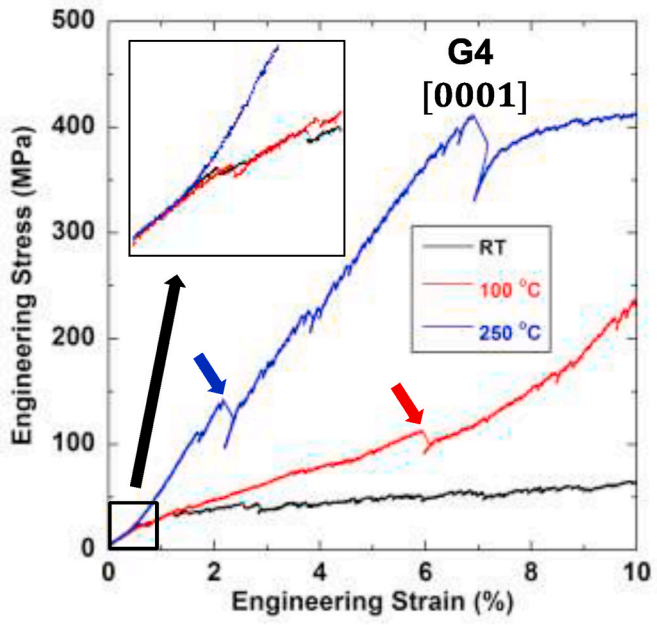

Fig. 9. Engineering stress-strain curves of micropillars at RT, 100 °C and 250 °C in G4.

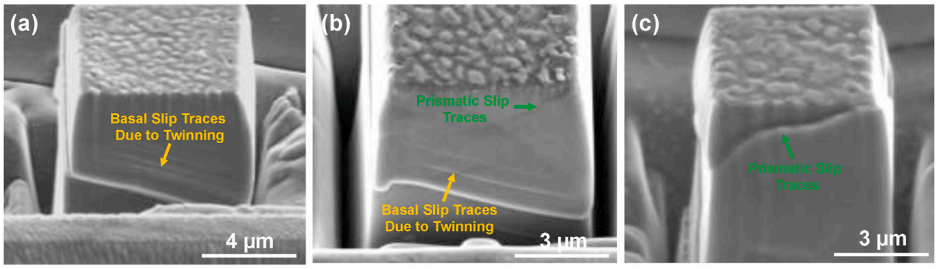

Fig. 8. Slip trace analysis of the micropillars in G3 that were compressed (a) RT, (b) 100 °C, (c) 250 °C.

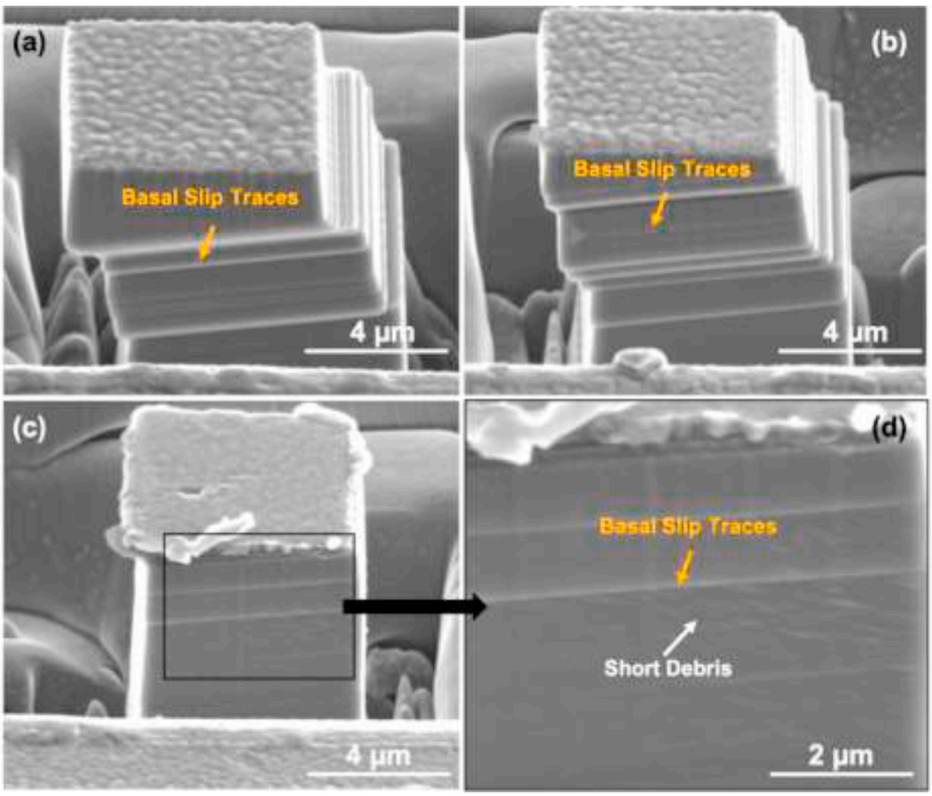

Fig. 10. Deformed micropillars at (a) RT, (b) 100 °C, (c, d) 250 °C in G4.

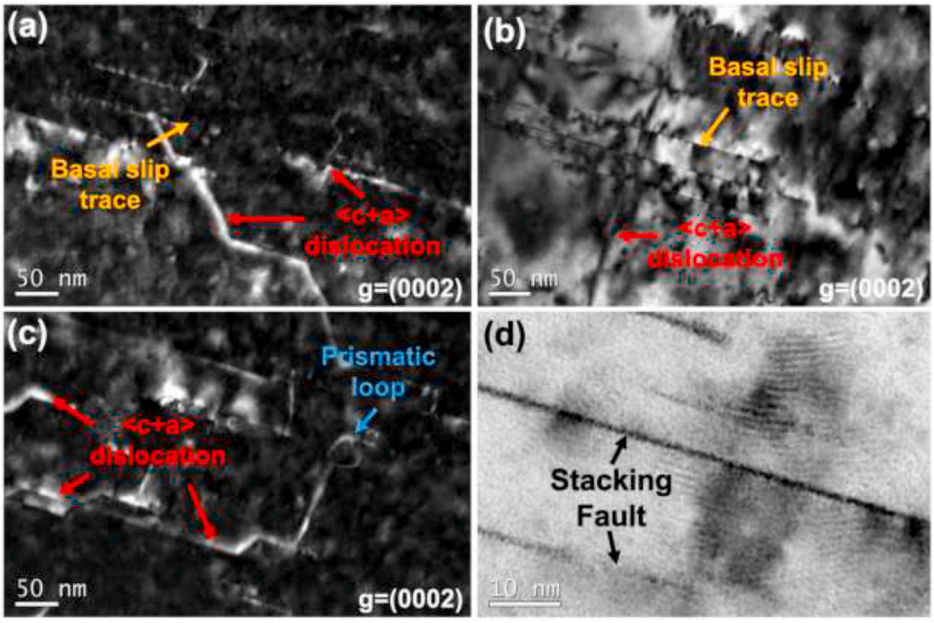

Fig. 11. TEM characterization of G4 micropillar compressed at 250 °C: (a–c) dislocation activity at $\bar{g} = (0002)$; (d) stacking faults formed by dislocation dissociation.

pyramidal slip due to high m (0.49) at this orientation. The non-basal slip was successfully tracked at 250 °C where short debris emerged on the lateral surface of the deformed micropillar, Fig. 10(c–d). Interestingly, at this temperature an abnormal strengthening effect was observed, despite of the occurrence of basal slip at initial deformation stage. This phenomena was firstly reported in pure Mg, and was rationalized by decomposition of <c+a> dislocation due to pyramidal slip [32–34]:

$$\frac{1}{3}\left[11\bar{2}3\right] \rightarrow [0001] + \frac{1}{3}\left[10\bar{1}0\right] + SF_{(0001)} + \frac{1}{3}\left[01\bar{1}0\right] \quad (5)$$

Based on this equation, the $<c+a>$ dislocation was decomposed to the dislocation and the stacking fault (SF) along basal plane (0001) and the partial dislocation along $1/3[01\bar{1}0]$. Accordingly, abrupt stress burst occurred at higher stress level (≈110 MPa, blue arrow) at ≈2% applied strain.

The proposed dislocation activity was further verified by TEM characterization on the 250 °C deformed micropillar, as shown in Fig. 11. Large density <c+a> dislocations were observed in the microstructure with $g = (0002)$. The <c+a> dislocations were formed by activation of pyramidal slips at HT (100 °C and 250 °C), in accordance with the observed short debris feature (Fig. 10d). The <c+a> dislocations were entangled with the <a> dislocations formed due to basal slip, leading to the strong work hardening behavior of this orientation at HT (Fig. 9). Note prismatic loops and SFs along basal plane were also observed, Fig. 11(c–d). Both microstructural features were formed by decomposition of the <c+a> dislocations at 250 °C. Based on Ref [35], the SFs are preferential spots to accommodate Y segregation (Suzuki segregation). Therefore, except for the dislocation decomposition, Y segregation is another mechanism leading to the abnormal strengthening of this orientation at 250 °C. The TEM observation supports strongly the activation of pyramidal slips, except for the basal slips at HT. Therefore, the observed stress burst at 100 °C and 250 °C must be correlated to the activation of pyramidal slip. Based on the critical stress level, the τ_{CRSS} for pyramidal slip was 43.7 ± 0.3 MPa at 100 °C and 45.6 ± 0.7 MPa at 250 °C, as listed in Table 2. Note both values are higher than the raw τ_{CRSS} in pure Mg at the same temperature (≈40 MPa at 100 °C and ≈20 MPa at 250 °C) [10]. The comparable values further suggest an enhanced temperature resistance of pyramidal slip in Mg–Y alloys.

4. Conclusions

In this work, micropillar compression was utilized to elucidate the microscale deformation mechanisms of basal slip, twinning and non-basal slips in a Mg-2 wt.% Y (Mg–2Y) at room temperature (RT) and high temperatures (100 °C and 250 °C). Based on the acquired stress-strain curves, the corresponding critical resolved shear stress (τ_{CRSS}) of individual slip mode was finally determined. Based on the studies, the following main conclusions can be drawn:

1. As measured at $[11\bar{2}3]$ and $[10\bar{1}0]$ orientations, the τ_{CRSS} for basal slip in Mg–2Y alloy was measured 12.5 ± 1.7 MPa, and that for twinning nucleation and growth 38.5 ± 1.2 MPa and 33.8 ± 0.7 MPa, respectively. The values were much higher than those reported in pure Mg, and suggests a more balanced deformation in the Mg–2Y alloy. Note the twinning favorable orientation showed a strong work hardening behavior upon micropillar compression, and this is a consequence of activation of <c+a> dislocations in the twinned orientation.
2. At prismatic-slip favorable orientation $[11\bar{2}0]$, the micropillar was deformed mainly by twinning at RT. Twinning-to-prismatic slip transition was observed at HT. Specially, at 250 °C, twinning was completely prohibited, and pure prismatic slip was triggered. The measured τ_{CRSS} for prismatic slip at 250 °C was 39.7 ± 0.3 MPa, much higher than that for pure Mg at th same temperature. This suggests a further strengthening effect in Mg–2Y alloy, especially at HT.
3. At pyramidal-slip favorable orientation [0001], pyramidal slips were triggered at 100 °C and 250 °C, following the basal slips, which led to an abnormal strengthening effect at HT. Detailed dislocation analysis further suggests an HT strengthening mechanism related to dislocation decomposition and Y segregation at stacking faults. The τ_{CRSS} for pyramidal slip was measured 43.7 ± 0.3 MPa at 100 °C and 45.6 ± 0.7 MPa at 250 °C. The comparable values further suggest an enhanced temperature resistance of pyramidal slip in Mg–Y alloys.

CRediT authorship contribution statement

Na Li: Investigation, Visualization, Writing – original draft. **Lingwei Yang:** Methodology, Formal analysis, Writing – review & editing. **Chuanyun Wang:** Investigation. **M.A. Monclús:** Methodology. **Dongfeng Shi:** Investigation. **J.M. Molina-Aldareguía:** Conceptualization, Supervision, Funding acquisition.

Declaration of competing interest

The authors declare that they have no known competing financial interests or personal relationships that could have appeared to influence the work reported in this paper.

Acknowledgements

The research leading to these results has received funding from the Madrid Region under programme [Grant Number S2013/MIT-2775], DIMMAT project (Spain). The authors (Na Li, Chuanyun Wang, Dongfeng Shi) are grateful to the China Scholarship Council (grant number: 201506020081; 201406290011; 201706050154) for financial support.

Appendix A. Supplementary data

Supplementary data to this article can be found online at https://doi.org/10.1016/j.msea.2021.141408.

References

[1] B.L. Mordike, T. Ebert, Magnesium properties - applications - potential, Mater. Sci. Eng. A. 302 (2001) 37–45.
[2] A.A. Luo, Magnesium : current and potential automotive applications, JOM 54 (2002) 42–48.
[3] M.K. Kulekci, Magnesium and its alloys applications in automotive industry, Int. J. Adv. Manuf. Technol. 39 (2008) 851–865.
[4] C.H. Caceres, Economical and environmental factors in light alloys automotive applications, Metall. Mater. Trans. 38 (2007) 1649–1662.
[5] M.P. Staiger, A.M. Pietak, J. Huadmai, G. Dias, Magnesium and its alloys as orthopedic biomaterials : a review, Biomaterials 27 (2006) 1728–1734.
[6] H. Yoshinaga, R. Horiuchi, Deformation mechanisms in magnesium single crystals compressed in the direction parallel to hexagonal axis, Trans. JIM. 4 (1963) 1–8.
[7] H. Conrad, W.D. Robertson, Effect of temperature on the flow stress and strain-hardening coefficient of magnesium single crystals, JOM 9 (1957) 503–512.
[8] E.C. Burke, W.R. Hibbard, Plastic deformation of magnesium single crystals, JOM 4 (1952) 295–303.
[9] J.F. Stohr, J.P. Poirier, Etude en microscopie electronique du glissement pyramidal {1122} <1123> dans le magnesium, Philos. Mag. A 25 (1972) 1313–1329.
[10] T. Obara, H. Yoshinga, S. Morozumi, {112¯2}S⟨1123⟩lip system in magnesium, Acta Metall. 21 (1973) 845–853.
[11] R.E. Reed-Hill, W.D. Robertson, Deformation of magnesium single crystals by nonbasal slip, JOM 9 (1957) 496–502.
[12] H. Zhang, Y. Liu, J. Fan, H.J. Roven, W. Cheng, B. Xu, H. Dong, Microstructure evolution and mechanical properties of twinned AZ31 alloy plates at lower elevated temperature, J. Alloys Compd. 615 (2014) 687–692.
[13] K.E. Prasad, K. Rajesh, U. Ramamurty, Micropillar and macropillar compression responses of magnesium single crystals oriented for single slip or extension twinning, Acta Mater. 65 (2014) 316–325.
[14] G.-D. Sim, K.Y. Xie, K.J. Hemker, J.A. El-Awady, Effect of temperature on the transition in deformation modes in Mg single crystals, Acta Mater. 178 (2019) 241–278.
[15] S. Sandlöbes, S. Zaefferer, I. Schestakow, S. Yi, R. Gonzalez-Martinez, On the role of non-basal deformation mechanisms for the ductility of Mg and Mg-Y alloys, Acta Mater.. 59(2), 429-439.
[16] X. Xia, Q. Chen, J. Li, D. Shu, C. Hu, S. Huang, Z. Zhao, Characterization of hot deformation behavior of as-extruded Mg-Gd-Y-Zn-Zr alloy, J. Alloys Compd. 610 (2014) 203–211.
[17] R. Sánchez-Martín, C. Zambaldi, M.T. Pérez-Prado, J.M. Molina-Aldareguia, High temperature deformation mechanisms in pure magnesium studied by nanoindentation, Scripta Mater. 104 (2015) 9–12.
[18] R. Sánchez-Martín, M.T. Pérez-Prado, J.J. Segurado, J.M. Molina-Aldareguia, Effect of indentation size on the nucleation and propagation of tensile twinning in pure magnesium, Acta Mater. 93 (2015) 114–128.
[19] G.S. Kim, Small Volume Investigation of Slip and Twinning in Magnesium Single Crystals, University of Grenoble, 2011. PhD thesis.
[20] Q. Yu, Size-related Mechanical Properties of Pure Magnesium, 2012. PhD thesis, UC Berkeley.
[21] J.-Y. Wang, N. Li, R. Alizadeh, M.A. Monclús, Y.W. Cui, J.M. Molina-Aldareguía, J. LLorca, Effect of solute content and temperature on the deformation mechanisms and critical resolved shear stress in Mg-Al and Mg-Zn alloys, Acta Mater. 170 (2019) 155–165.
[22] Q. Yu, Z. Shan, J. Li, X. Huang, L. Xiao, J. Sun, E. Ma, Strong Crystal Size Effect on Deformation Twinning, vol. 463, 2010, pp. 335–338.

[23] I.N. Sneddon, The relation between load and penetration in the axisymmetric Boussinesq problem for a punch of arbitrary profile, Int. J. Eng. Sci. 3 (1965) 47–57.
[24] J.R. Greer, W.C. Oliver, W.D. Nix, Size dependence of mechanical properties of gold at the micron scale in the absence of strain gradients, Acta Mater. 53 (2005) 1821–1830.
[25] S.R. Agnew, M.H. Yoo, C.N. Tomé, C.N. Tome, Application of texture simulation to understanding mechanical behavior of Mg and solid solution aloy containning Li or Y, Acta Mater. 49 (2001) 4277–4289.
[26] A. Tehranchi, B. Yin, W.A. Curtin, Solute strengthening of basal slip in Mg alloys, Acta Mater. 151 (2018) 56–66.
[27] Y. Liu, N. Li, M. Arul Kumar, S. Pathak, J. Wang, R.J.J. McCabe, N.A.A. Mara, C.N. N. Tomé, Experimentally quantifying critical stresses associated with basal slip and twinning in magnesium using micropillars, Acta Mater. 135 (2017) 411–421.
[28] J. Wang, N. Stanford, Investigation of precipitate hardening of slip and twinning in Mg5 % Zn by micropillar compression, Acta Mater. 100 (2015) 53–63.
[29] J. Wang, J.M. Molina-Aldareguía, J. LLorca, Effect of Al content on the critical resolved shear stress for twin nucleation and growth in Mg alloys, Acta Mater. 188 (2020) 215–227.
[30] S.Y. Chang, T. Nakagaido, S.K. Hong, D.H. Shin, T. Sato, Effect of yttrium on high temperature strength of magnesium, Mater. Trans. 42 (2001) 1332–1338.
[31] A. Singh, Tailoring microstructure of Mg-Zn-Y alloys with quasicrystal and related phases for high mechanical strength, Sci. Technol. Adv. Mater. 15 (2014), 044803.
[32] H. Yoshinaga, R. Horiuchi, On the nonbasal slip in crystals *, Trans. J I M. 5 (1964) 14–21.
[33] S.R. Agnew, L. Capolungo, C.A. Calhoun, Connections between the basal I1 "growth" fault and <c + a> dislocations, Acta Mater. 82 (2015) 255–265.
[34] B. Yin, Z. Wu, W.A. Curtin, First-principles calculations of stacking fault energies in Mg-Y, Mg-Al and Mg-Zn alloys and implications for <c + a> activity, Acta Mater. 136 (2017) 249–261.
[35] J. Koike, T. Kobayashi, T. Mukai, H. Watanabe, M. Suzuki, The activity of non-basal slip systems and dynamic recovery at room temperature in fine-grained, AZ31B magnesium alloys 51 (2003) 2055–2065.